Wave Motion 120 (2023) 103138

Contents lists available at ScienceDirect

Wave Motion

journal homepage: www.elsevier.com/locate/wamot

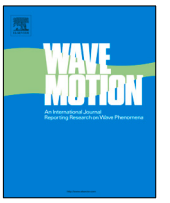

Ultrasonic wave propagation in randomly layered heterogeneous media

Alistair S. Ferguson [a,*], Anthony J. Mulholland [b], Katherine M.M. Tant [a], Mohammud Foondun [a]

[a] Department of Mathematics and Statistics, University of Strathclyde, Glasgow, G1 1XH, United Kingdom
[b] Department of Engineering Mathematics, University of Bristol, Bristol, BS8 1QU, United Kingdom

ARTICLE INFO

Article history:
Received 1 June 2021
Received in revised form 14 February 2023
Accepted 15 March 2023
Available online 3 April 2023

Keywords:
Wave propagation in random media
Stochastic differential equations
Anisotropy
Multiple scattering
Diffusion approximation

ABSTRACT

This article considers the propagation of high frequency elastic waves in a layered material. Each layer is locally anisotropic and the layer thicknesses and slowness surface orientations are modelled by a (Markovian) process. This work is important in deepening our understanding of the ultrasonic non-destructive testing of carbon fibre reinforced polymer (CFRP) composites and polycrystalline materials. The paper focuses on monochromatic shear waves propagating in two-dimensional ((x_1, x_3) plane) heterogeneous media. The displacement is in the x_2 direction and the model focuses on the reflection and transmission of the wave at layer interfaces. The rotation of the slowness surface in each layer lies in the (x_1, x_2) plane and varies with the wave propagation direction (x_3) only. Expressions for the local and global coefficients for the reflected and transmitted wave amplitudes are derived and shown to satisfy energy conservation. The resulting stochastic differential equations lead to a self-adjoint infinitesimal generator which can be used to produce a Fokker–Planck equation to study the probability distribution of the transmission coefficient. Explicit expressions for the moments of the probability distributions of the power transmission and reflection coefficients are then derived. The dependency of the mean and standard deviation of the power transmission coefficient on the depth of wave penetration, the localisation length, and the direction of wave propagation is then reported.

1. Introduction

Ultrasonic non-destructive evaluation (NDE) is an important technique for assessing the structural integrity of industrial infrastructure. It involves sending mechanical waves through the object of interest and analysing the resulting scattered field to determine if there exists any embedded defects [1]. It is common practice when performing NDE on an unknown material to assume homogeneous material properties [2]. However, this is a physically unrealistic assumption in many materials of interest (for example austenitic steel) [3]. Wavelength size structures exist in many industrial materials which can lead to significant multiple scattering and the medium not being well characterised using homogenisation [2]. Waves propagating through such heterogeneous media experience scattering that attenuates the coherent input wave and transfers energy to small incoherent fluctuations [4]. A deterministic approach to studying horizontally polarised shear waves was reported in [5] where the symmetry axis of rotation was out of plane (where an austenitic steel weld

* Corresponding author.
E-mail address: alistair@bosonmail.com (A.S. Ferguson).

https://doi.org/10.1016/j.wavemoti.2023.103138

was analysed) but with no consideration for random fluctuations in the wave amplitude produced by scattering from interactions with the internal material microstructure.

Recent studies using numerical simulations have outlined the effects of internal material microstructures on beam propagation. When the size of the internal grain microstructure is commensurate with the wavelength, amplitude fluctuations can be observed in the transmitted and repeated waveforms [6]. If these factors are ignored, deterministic models of wave propagation can give a poor representation of the transmitted and reflected waves and this in turn can negatively affect our ability to reliably detect and resolve flaws. Understanding such phenomena is key to developing NDE imaging methods based on the incoherent waves (coda waves) that result from ultrasonic wave propagation in such materials. Elastic wave propagation in anisotropic solids is also important in medical imaging [7] and in migration problems in geophysics [8] where time reversal techniques are of interest.

In this paper, we wish to study length scale regimes where the received wave is complex, exhibiting many fluctuations over a long time period caused by its convoluted journey through the heterogeneous layered medium. The random medium is embedded between two homogeneous half spaces with a unit wave impinging at $x_3 = 0$. In this case, the input wave (which is a horizontally polarised shear wave) is so affected by its interactions with the medium that a homogenisation approach is inappropriate. This can occur when the propagation distance L is much larger than the wavelength (λ_3) of propagation which in turn is much larger than the layer sizes l ($L \gg \lambda_3 \gg l$) and the fluctuations in the material are large ($\sigma \sim 1$); the so called *strongly* heterogeneous regime [9]. It can also occur in the regime where $L_3 \gg \lambda_3 \sim l$ and $\sigma \ll 1$, which is the so called *weakly* heterogeneous regime and it is this latter case that will be examined in this paper.

The decay of a coherent wave has been studied in the literature for general acoustic and elastic systems. Articles [9–11] consider acoustic systems in one dimension and more recently [4,12] considered elastic media, where the latter addressed three-dimensional random media in a different scaling regime than is presented in this paper. In each case, stochastic differential equations (SDE's) arise due to the modelling assumptions for the random fluctuations in the material properties [13]. Each of these studies examined a wave travelling in a medium whose properties only varied in the direction of propagation, leading to a system of stochastic differential equations satisfied by a propagator matrix with certain symmetry properties. This paper uses a similar approach to consider a shear wave propagating in an elastic medium with random fluctuations in the material microstructure. As far as the authors are aware, this is the first time that the direction of wave propagation has been incorporated into this methodology for elastodynamic waves. Current NDE practice involves the use of an array of transmitting/receiving elements so that the direction and focus of the emitted wave can be adjusted [14], and so understanding how this change in wave direction interacts with a layered medium is therefore of significant interest. The effect that the localisation length and the direction of the monochromatic shear wave has on the attenuation of the transmitted wave, is studied.

The paper can be summarised as follows. Section 2 introduces the governing elastodynamic equations where the wave parameterisation is chosen and the resulting evolution equations are derived. Section 3 introduces the stochastic process governing the fluctuations in the material parameters in the form of a randomly varying slowness surface angle. We also non-dimensionalise the equations in this Section and formulate a random forward–backward wave mode equation. Section 4 introduces the weakly heterogeneous scaling regime which is appropriate for the study of ultrasonic waves in the non-destructive testing of austenitic steel welds. A diffusion approximation is used to derive a tractable system of SDE"s which is solved to obtain a Fokker–Planck equation for the probability density function of the transmitted energy in Section 4.4. Sections 4.4 and 4.5 follow closely the analysis presented in [9] (Ch. 7). Section 5 contains some numerical results showing the dependency of the mean and standard deviation of the power transmission coefficient for ultrasonic wave propagation in austenitic steel.

2. Governing equations

We are interested in studying waves in a host medium composed of just one anisotropic material. The media is partitioned into layers and the orientation of the material varies from one layer to the next. Since the material is anisotropic, this variation in orientation affects the speed at which the incident wave travels through each region and hence the wave experiences a change in mechanical impedance and therefore a spatially heterogeneous medium. This local variation in wave speed can be described using a slowness curve which can be derived analytically from the Christoffel equation [15]. The governing elastic wave equation can be written

$$\rho \frac{\partial^2 u_i}{\partial t^2} = \sum_{k=1}^{3} \frac{\partial \tau_{ik}}{\partial x_k}, \quad i = 1, 2, 3, \quad \mathbf{u}(t, \mathbf{x}) : \mathbb{R}^+ \times \mathbb{R}^3 \to \mathbb{R}^3, \quad \tau_{ik}(t, \mathbf{x}) : \mathbb{R}^+ \times \mathbb{R}^3 \to \mathbb{R}^{3\times 3}, \tag{1}$$

where the displacement vector is denoted $\boldsymbol{u} = (u_1(t, \boldsymbol{x}), u_2(t, \boldsymbol{x}), u_3(t, \boldsymbol{x}))$, ρ is the density of the material (assumed to be constant) and τ_{jk} is the material stress tensor. The material is contained in $x_3 \in [0, L]$, where L is the width of the media. Denoting $\boldsymbol{s} = (s_1, s_2, s_3)$ the symmetry axis vector in two dimensions (the (x_1, x_2) plane) defined by

$\boldsymbol{s} = [\cos\theta(x_3), \sin\theta(x_3), 0]^T$, the stiffness tensor can be written [16] as

$$\begin{aligned} c_{ijkl} =& (A-2N)\delta_{ij}\delta_{kl} + N\left(\delta_{ik}\delta_{jl} + \delta_{il}\delta_{jk}\right) \\ &+ (F - A + 2N)\left(\delta_{ij}s_k s_l + \delta_{kl}s_i s_j\right) \\ &+ (S-N)\left(\delta_{ik}s_j s_l + \delta_{il}s_j s_k + \delta_{jk}s_i s_l + \delta_{jl}s_i s_k\right) \\ &+ (A + C - 2F - 4S)s_i s_j s_k s_l. \end{aligned} \tag{2}$$

Note that $A = C_{33}$, $C = C_{11}$, $F = C_{13}$, $N = C_{44}$, $S = C_{66}$ when $\theta = 0$, so the stiffness matrix has the form in [17] when the symmetry axis points in the x_1 direction. The stiffness tensor for a transversely isotropic medium has five independent components denoted (in Voigt notation) C_{11}, C_{33}, C_{13}, C_{66} and C_{44}. This form assumes that the anisotropy is spatially varying only in the x_3 direction as in [9]. However, in [9], $\boldsymbol{s}$ lies in the (x_1, x_3) plane but here it lies in the (x_1, x_2) plane, making an angle $\theta(x_3)$ with the x_1 axis as shown in Fig. 1. We restrict attention to the case of a shear wave with the displacement vector remaining in the x_2 direction when the wave propagates through the random medium. It is important to note that the displacement vector remains in the x_2 plane when the wave propagates through the random medium. The elastic tensor relates the symmetric strain and stress tensors via Hooke's law

$$\tau_{ij} = \sum_{k,l=1}^{3} c_{ijkl}e_{kl}, \tag{3}$$

where the symmetric strain tensor is given by

$$e_{kl} = \frac{1}{2}\left(\frac{\partial u_k}{\partial x_l} + \frac{\partial u_l}{\partial x_k}\right). \tag{4}$$

Consider a horizontally polarised shear wave [5] with displacement vector

$$(u_j)_{j=1}^{3} = (0, u_2(x_1, x_3), 0), \tag{5}$$

whereby the medium vibrates in a direction perpendicular to the (x_1, x_3) plane. The velocity in the x_2 direction is defined as

$$\xi = \frac{\partial u_2}{\partial t} = u_{2,t}. \tag{6}$$

The wave direction is then in the (x_1, x_3) plane. Using this parameterisation (and moving to Voigt notation for convenience) Eq. (3) becomes

$$\tau_{21,t} = c_{66}\xi_{,1}, \tag{7}$$

$$\tau_{32,t} = c_{44}\xi_{,3}, \tag{8}$$

where

$$c_{66}(x_3) = S + (A + C - 2F - 4S)\cos^2(\theta(x_3))\sin^2(\theta(x_3)), \tag{9}$$

$$c_{44}(x_3) = N + (S-N)\sin^2(\theta(x_3)). \tag{10}$$

The elastic wave Eq. (1) can then be rewritten as

$$\rho\xi_{,t} = \tau_{21,1} + \tau_{32,3}. \tag{11}$$

At time $t = 0$, a source term excites the medium at $x_3 = 0$, and radiation conditions demand that the amplitude of the propagating wave tends to zero as $x \to \pm\infty$. Using positive sign convention, we take Fourier transforms in time and space (in the x_1 direction with respect to a wavenumber κ_1) of the stress and velocity equations; in this time-harmonic domain the stress and velocity are denoted by $\hat{\tau}$ and $\hat{\xi}$ respectively. Define the temporal Fourier transform of a function $f(t, x_1, x_3)$ by

$$\check{f}(\omega, x_1, x_3) = \int f(t, x_1, x_3)e^{i\omega t}dt, \tag{12}$$

where ω is the angular frequency. Define the spatial Fourier transform with respect to a wavenumber κ_1 in the x_1 direction by

$$\hat{f}(\omega, \kappa_1, x_3) = \int \check{f}(\omega, x_1, x_3)e^{i\kappa_1 x_1}dx_1. \tag{13}$$

Eqs. (11), (7) and (8) become

$$-\rho i\omega\hat{\xi}(\omega, \kappa_1, x_3) = -i\kappa_1\hat{\tau}_{21}(\omega, \kappa_1, x_3) + \hat{\tau}_{32,3}(\omega, \kappa_1, x_3), \tag{14}$$

$$-i\omega\hat{\tau}_{21}(\omega, \kappa_1, x_3) = -i\kappa_1 c_{66}\hat{\xi}(\omega, \kappa_1, x_3), \tag{15}$$

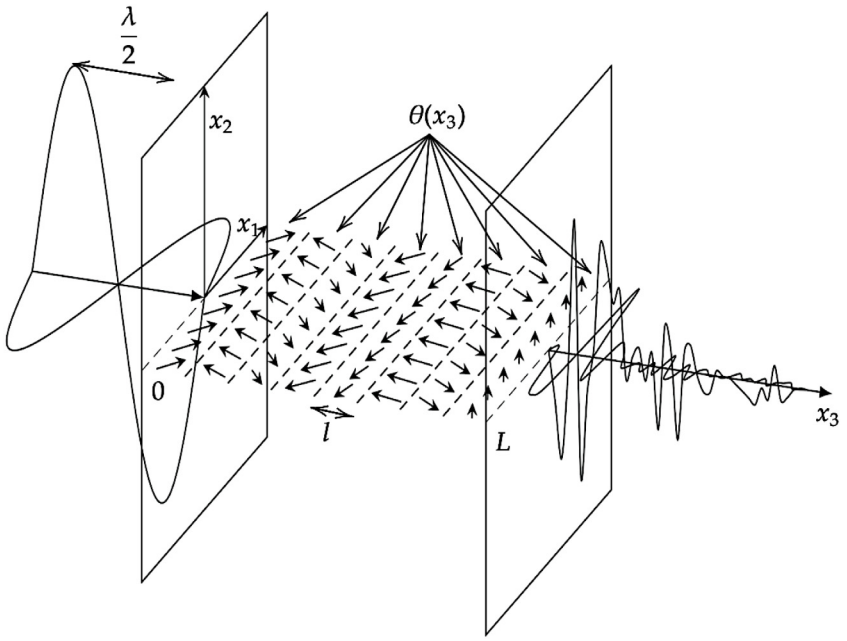

Fig. 1. For each value of $x_3 \in [0, L_3] \subseteq \mathbb{R}$, the material is anisotropic in the (x_1, x_2) plane. The degree of anisotropy is dictated by the material's slowness surface and $\theta(x_3)$ describes its rotation in the (x_1, x_2) plane. The direction of wave propagation is fixed and lies in the (x_1, x_3) plane. In each layer (shown by the dashed lines) the material properties are constant. At $x_3 = 0$ we show an elastic shear wave with wavelength λ incident on a randomly layered material with layer size l and slab length L. The small arrows indicate the local crystal orientation $\theta(x_3)$ (the symmetry axis vector and hence θ, lie in the (x_1, x_2) plane) of the anisotropic material in each layer. Upon exiting the material the transmitted wave has very little energy in the coherent wave and has a long coda wave.

$$-i\omega\hat{\tau}_{32}(\omega, \kappa_1, x_3) = c_{44}\hat{\hat{\xi}}_{,3}(\omega, \kappa_1, x_3). \tag{16}$$

These can be rewritten in matrix form (the subscript 32 is dropped for notational convenience) to obtain a system of velocity and stress evolution equations

$$\frac{\partial}{\partial x_3}\begin{bmatrix}\hat{\hat{\xi}}(\omega, \kappa_1, x_3)\\ \hat{\tau}(\omega, \kappa_1, x_3)\end{bmatrix} = \begin{bmatrix}0 & -i\alpha\\ -i\beta & 0\end{bmatrix}\begin{bmatrix}\hat{\hat{\xi}}(\omega, \kappa_1, x_3)\\ \hat{\tau}(\omega, \kappa_1, x_3)\end{bmatrix}, \quad \hat{\hat{\xi}}(\omega, \kappa_1, x_3),\ \hat{\tau}(\omega, \kappa_1, x_3) : \mathbb{R}^3 \to \mathbb{R}, \tag{17}$$

where the boundary conditions are the radiation conditions whereby $\hat{\hat{\xi}} \to 0$ as $x_3 \to \pm\infty$ and $\hat{\tau} \to 0$ as $x_3 \to \pm\infty$, and a wave is initiated by imposing an initial stress $\hat{\tau}_0$ and velocity $\hat{\hat{\xi}}_0$ at $x_3 = 0$. Furthermore

$$\alpha = \frac{\omega}{c_{44}}, \tag{18}$$

and

$$\beta = \frac{\rho\omega^2 - \kappa_1^2 c_{66}}{\omega}, \tag{19}$$

where we assume that $\beta > 0$ and set $\zeta = \sqrt{\beta\alpha}$. For typical stiffness matrix values the spatially varying stiffness coefficient given by Eq. (9) is positive. So, if the incident wave is such that the phase velocity in the x_1 direction (ω/κ_1) exceeds the spatially varying velocity $\sqrt{c_{66}(x_3)/\rho}$ in the x_3 direction then the wave-field will satisfy this condition throughout the domain.

3. Randomly layered anisotropic medium

The stochastic model we employ to describe the heterogeneities gives rise to fluctuations which build up behind the pulse, producing a distorted coda wave exiting the material. We assume that the material is Markovian, the polycrystalline orientations from one layer to the next are independent and the layer sizes are independent from one layer to another; see [18] for an example. The heterogeneous nature of these materials is complex and to enable analytical headway this simplified model to describe the material fluctuations is used.

As the angle θ varies in the (x_1, x_2) plane, the stress tensor components of the material are given by Eqs. (9) and (10). We will assume that the angle $\theta(x_3)$ varies randomly over the interval $x_3 \in [0, L]$ according to

$$\theta(x_3) = \bar{\theta} + \sigma m(x_3/l), \quad x_3 \in [0, L]. \tag{20}$$

where $\bar{\theta} \sim 1$ is the mean angle, $m(x_3/l)$ is a stationary stochastic process (an ergodic Markov process on a compact state space, see Section 6.1.5 in [9]) with mean zero. The random process $m(x_3/l)$ takes values in $\mathbb{R}$, on an interval which is closed and bounded (typically m is drawn from a uniform distribution in the interval $[-1,1]$). Here l is a typical layer size inside the material and σ is a dimensionless and small parameter ($0 < \sigma \ll 1$) which controls the amplitude of the random fluctuations. To assist in the analysis that follows, we linearise this dependency of the material properties with respect to the random process $m(x_3/l)$. As such, the range of validity of the analysis is restricted to the regime where the governing equations are approximately linear with respect to $m(x_3/l)$; given the dependency on θ in Eqs. (21) and (22) this will be centred on $\bar{\theta} = \pi/8$. A Taylor expansion at first order (in σ) gives us

$$c_{66} = \bar{c}_{66}\Big(1 + \varphi m(x_3/l)\Big), \tag{21}$$

where $\bar{c}_{66} = S + \varrho \cos^2\bar{\theta}\sin^2\bar{\theta}$, $\varrho = A + C - 2F - 4S$ and $\varphi = \sigma\varrho\sin(2\bar{\theta})\cos(2\bar{\theta})/\bar{c}_{66}$. Similarly

$$c_{44} = \bar{c}_{44}\Big(1 + \vartheta m(x_3/l)\Big), \tag{22}$$

where $\bar{c}_{44} = N + (S - N)\sin^2\bar{\theta}$ and $\vartheta = \sigma(S - N)\sin(2\bar{\theta})/\bar{c}_{44}$. Eq. (18) is now

$$\alpha = \bar{\alpha}(1 - \vartheta m(x_3/l)), \tag{23}$$

where $\bar{\alpha} = \omega/\bar{c}_{44}$ and $\vartheta = -\sigma\Gamma_\alpha$, where

$$\Gamma_\alpha = \frac{(N - S)\sin(2\bar{\theta})}{\bar{c}_{44}}. \tag{24}$$

Eq. (19) can then be written

$$\beta = \bar{\beta}(1 + \varsigma m(x_3/l)), \tag{25}$$

where $\bar{\beta} = (\kappa_1^2\bar{c}_{66} - \rho\omega^2)/\omega$ and $\varsigma = (\bar{c}_{66}\varphi\kappa_1^2)/(\kappa_1^2\bar{c}_{66} - \rho\omega^2) = \sigma\Gamma_\beta$ where

$$\Gamma_\beta = \frac{\kappa_1^2\varrho\sin(2\bar{\theta})\cos(2\bar{\theta})}{\Big(\kappa_1^2\bar{c}_{66} - \rho\omega^2\Big)}. \tag{26}$$

Inserting (23) and (25) into the stress-velocity evolution (17) gives

$$\frac{\partial}{\partial x_3}\begin{bmatrix}\hat{\xi}(\omega,\kappa_1,x_3)\\ \hat{\tau}(\omega,\kappa_1,x_3)\end{bmatrix} = \begin{bmatrix}0 & -i\bar{\alpha}(1 - \vartheta m(x_3/l))\\ i\bar{\beta}(1 + \varsigma m(x_3/l)) & 0\end{bmatrix}\begin{bmatrix}\hat{\xi}(\omega,\kappa_1,x_3)\\ \hat{\tau}(\omega,\kappa_1,x_3)\end{bmatrix}, \tag{27}$$

where $\hat{\xi}(\omega,\kappa_1,x_3) : \mathbb{R}^+\times\mathbb{R}^+\times\mathbb{R} \to \mathbb{R}$ and $\hat{\tau}(\omega,\kappa_1,x_3) : \mathbb{R}^+\times\mathbb{R}^+\times\mathbb{R} \to \mathbb{R}$. The incident velocity and stress are prescribed at $x_3 = 0$ and the boundary conditions are in the form of radiation conditions such that the stress and velocity tend to zero as x_3 tends to $\pm\infty$.

3.1. The dimensionless elastic wave equations

To put the system of governing equations (27) in a dimensionless form, we choose the dimensionless variables

$$\tilde{x}_3 = \frac{x_3}{L_3}, \quad \tilde{\omega} = \frac{L_3\,\omega}{c_3}, \quad \text{and} \quad \tilde{\kappa}_1 = \kappa_1 L_3, \tag{28}$$

where L_3 is a typical propagation distance in x_3 and c_3 is the mean wave speed in the x_3 direction. We can interpret $\tilde{x}_3$ as a ratio of distances in the propagation direction, $\tilde{\omega}$ as a ratio of the propagation distance to the typical wavelength in the propagation direction and $\tilde{\kappa}_1$ as a ratio of propagation distance per wavelength in the x_1 direction. We define two dimensionless parameters ε and ϖ in order to capture the length scale differences in the problem via

$$\varepsilon \ll 1, \quad \frac{L_3}{l} = \frac{1}{\varepsilon^2}, \quad \text{and} \quad \varpi = \varepsilon\tilde{\omega}, \tag{29}$$

where ε is ($0 < \varepsilon \ll 1$) in the weakly heterogeneous regime (see [9] where the same analysis is followed but for the acoustic wave case). These relations can be combined to give

$$\varepsilon = \sqrt{\frac{l}{L_3}}, \quad \text{and} \quad \varpi = \frac{\omega}{c_3}\sqrt{lL_3}. \tag{30}$$

From Eq. (27) the non-dimensional stress and velocity equations read

$$\frac{\partial}{\partial\tilde{x}_3}\begin{bmatrix}\tilde{\xi}\\ \tilde{\tau}\end{bmatrix} = \begin{bmatrix}0 & -i(\tilde{\omega}/\bar{c}_{44})(1 - \vartheta m(\tilde{x}_3/\varepsilon^2))\\ i\tilde{\omega}((\tilde{\kappa}_1^2/\tilde{\omega}^2)\bar{c}_{66} - 1)(1 + \varsigma m(\tilde{x}_3/\varepsilon^2)) & 0\end{bmatrix}\begin{bmatrix}\tilde{\xi}\\ \tilde{\tau}\end{bmatrix}, \tag{31}$$

where $\tilde{c}_{44} = \bar{c}_{44}/(\rho c_3^2)$ and $\tilde{c}_{66} = \bar{c}_{66}/(\rho c_3^2)$. Let us define ν via

$$\tilde{\kappa}_1 = \nu\tilde{\omega}, \tag{32}$$

where

$$\nu = \frac{\tilde{\kappa}_1}{\tilde{\omega}} = \frac{\kappa_1 L_3}{(L_3\omega/c_3)} = \frac{\kappa_1}{\kappa_3}, \tag{33}$$

is the ratio of wave numbers in the $(x_1,\ x_3)$ directions. As such, ν is related to the direction of wave propagation in the $(x_1,\ x_3)$ plane. Hence, Eq. (31) becomes

$$\frac{\partial}{\partial\tilde{x}_3}\begin{bmatrix}\tilde{\xi}(\tilde{\omega},\tilde{\kappa_1},\tilde{x_3})\\ \tilde{\tau}(\tilde{\omega},\tilde{\kappa_1},\tilde{x_3})\end{bmatrix} = i\frac{\varpi}{\varepsilon}\begin{bmatrix}0 & d_1(1+\sigma\Gamma_\alpha m(\tilde{x}_3/\varepsilon^2))\\ d_2(1+\sigma\Gamma_\beta m(\tilde{x}_3/\varepsilon^2)) & 0\end{bmatrix}\begin{bmatrix}\tilde{\xi}(\tilde{\omega},\tilde{\kappa_1},\tilde{x_3})\\ \tilde{\tau}(\tilde{\omega},\tilde{\kappa_1},\tilde{x_3})\end{bmatrix} \tag{34}$$

where $d_1 = -1/\tilde{c}_{44}$, $d_2 = \nu^2\tilde{c}_{66} - 1$ and Eqs. (26) and (33) give

$$\Gamma_\beta = \frac{\nu^2\varrho\sin(2\bar{\theta})\cos(2\bar{\theta})}{\nu^2\bar{c}_{66} - \rho c_3^2}. \tag{35}$$

Letting

$$\hat{\xi}(\omega,\kappa_1,x_3) = \hat{a}(\omega,\kappa_1,x_3)e^{i\varpi/\varepsilon\sqrt{d_1d_2}x_3} + \hat{b}(\omega,\kappa_1,x_3)e^{-i\varpi/\varepsilon\sqrt{d_1d_2}x_3}, \tag{36}$$

and

$$\hat{\tau}(\omega,\kappa_1,x_3) = \sqrt{d_2/d_1}\left(\hat{a}(\omega,\kappa_1,x_3)e^{i\varpi/\varepsilon\sqrt{d_1d_2}x_3} - \hat{b}(\omega,\kappa_1,x_3)e^{-i\varpi/\varepsilon\sqrt{d_1d_2}x_3}\right), \tag{37}$$

(dropping tildes) Eq. (34) becomes ($\hat{a}$, $\hat{b}$ are right and left-going wave moves respectively)

$$\frac{\partial}{\partial x_3}\begin{bmatrix}\hat{a}\\ \hat{b}\end{bmatrix} = \frac{i\varpi\sigma}{2\varepsilon}m(x_3/\varepsilon^2)\begin{bmatrix}\sqrt{d_1d_2}(\Gamma_\alpha+\Gamma_\beta) & \sqrt{d_1d_2}(\Gamma_\beta-\Gamma_\alpha)e^{-2i\frac{\varpi}{\varepsilon}\sqrt{d_1d_2}x_3}\\ \sqrt{d_1d_2}(\Gamma_\alpha-\Gamma_\beta)e^{2i\frac{\varpi}{\varepsilon}\sqrt{d_1d_2}x_3} & -\sqrt{d_1d_2}(\Gamma_\alpha+\Gamma_\beta)\end{bmatrix}\begin{bmatrix}\hat{a}\\ \hat{b}\end{bmatrix}, \tag{38}$$

a system of scaled dimensionless wave-mode evolution equations, where $\hat{a}(\omega,\kappa_1,x_3) : \mathbb{R}^+\times\mathbb{R}^+\times\mathbb{R}\to\mathbb{R}$ and $\hat{b}(\omega,\kappa_1,x_3) : \mathbb{R}^+\times\mathbb{R}^+\times\mathbb{R}\to\mathbb{R}$. The initial conditions are that $\hat{a}(\omega,\kappa_1,x_3)$ and $\hat{b}(\omega,\kappa_1,x_3)$ are prescribed at $x_3 = 0$ and the radiation conditions are such that $\hat{a}$ and $\hat{b}$ tend to zero as x_3 tends to $\pm\infty$.

4. The weakly heterogeneous regime

The weakly heterogeneous regime is a high frequency regime (wavelength λ_3 is small relative to the slab length L_3, but commensurate with the microscopic layer length l) where the amplitude of the fluctuations in the medium properties is weak. The strength of the random fluctuations in Eq. (20) is controlled by σ where $0 < \sigma \ll 1$. The propagation distance is large so that significant multiple scattering occurs. For certain manufactured layered materials (such as a CFRP or an additively manufactured polycrystalline metals) there is a need to detect flaws using ultrasound waves. There is a trade-off between the resolution that can be achieved and the depth of penetration of the ultrasound wave due to the multiple scattering of the wave by the layered structure. These materials typical adhere to the weakly heterogeneous scaling regime studied in this paper. The ratio of wavenumbers (captured by the parameter ν) and the frequency of the ultrasound wave dictate the depth of wave penetration and the wavelength dictates the spatial resolution of the ultrasound imaging algorithm. The model presented here (via the localisation length) can be used by ultrasound engineers to decide on the optimal frequency of operation/design of the ultrasound sensor for a particular non-destructive testing application. This regime corresponds to $L_3 \gg \lambda_3 \sim l$, $0 < \sigma \ll 1$, where λ_3 is the wavelength in the x_3 direction. From Eq. (29)

$$1 \ll \frac{L_3}{\lambda_3} = \frac{\omega L_3}{2\pi c_3} = \frac{\tilde{\omega}}{2\pi} = \frac{\varpi}{2\pi\varepsilon}, \tag{39}$$

and from Eq. (30)

$$\frac{l}{\lambda_3} = \frac{\omega l}{2\pi c_3} = \frac{\omega L_3}{2\pi c_3}\frac{l}{L_3} = \frac{\varpi}{2\pi\varepsilon}\varepsilon^2 = \frac{\varpi\varepsilon}{2\pi} \sim 1. \tag{40}$$

Eq. (40) implies (with $0 < \varepsilon \ll 1$) that

$$\varpi \sim \frac{1}{\varepsilon}, \tag{41}$$

and so Eq. (39) holds and since $0 < \sigma \ll 1$ then we set $\sigma = \varepsilon$. Recall from Eq. (32) that we have normalised our random and dimensionless linear system, enabling us to apply a diffusion approximation (following Theorem 6.5, Section 6.5.2 [9]). Whilst the diffusion approximation theory can deal with more general cases, the linearisation (which is justified in this setting) enables more analytical headway to be made. Eqs. (29) and (41) imply that $\tilde{\omega} \sim \varepsilon^{-2}$. These parameter

choices ensure that the material fluctuation amplitude σ, is small, the layer size l is much smaller than the propagation distance L_3, the system is in a high frequency regime $L_3 \gg \lambda_3$, and the propagation distance is large enough so the wave experiences significant scattering $L_3 \sim L_{loc}$ (L_{loc} is the localisation length [9] which is given explicitly later in Eq. (80)). In this scaling regime the evolution Eq. (38) reads

$$\frac{d}{dx_3}\begin{bmatrix}\hat{a}^\varepsilon\\ \hat{b}^\varepsilon\end{bmatrix} = \frac{1}{\varepsilon}\mathbf{H}\left(\frac{x_3}{\varepsilon^2}, m\left(\frac{x_3}{\varepsilon^2}\right)\right)\begin{bmatrix}\hat{a}^\varepsilon\\ \hat{b}^\varepsilon\end{bmatrix}, \tag{42}$$

where

$$\mathbf{H}\left(\frac{x_3}{\varepsilon^2}, m\left(\frac{x_3}{\varepsilon^2}\right)\right) = \frac{im(x_3/\varepsilon^2)}{2}\begin{bmatrix}\delta_1 & -\delta_2 e^{-i\frac{\phi x_3}{\varepsilon^2}}\\ \delta_2 e^{i\frac{\phi x_3}{\varepsilon^2}} & -\delta_1\end{bmatrix}, \tag{43}$$

$\hat{a}^\varepsilon(\omega,\kappa_1,x_3) : \mathbb{R}^+\times\mathbb{R}^+\times\mathbb{R}\to\mathbb{R}$ and $\hat{b}^\varepsilon(\omega,\kappa_1,x_3) : \mathbb{R}^+\times\mathbb{R}^+\times\mathbb{R}\to\mathbb{R}$. The initial conditions are such that at $\hat{a}^\varepsilon$ and $\hat{b}^\varepsilon$ are prescribed at $x_3 = 0$ and the radiation conditions demand that $\hat{a}^\varepsilon$ and $\hat{b}^\varepsilon$ tend to zero as x_3 tends to $\pm\infty$. Here $\delta_1 = \sqrt{d_1 d_2}(\Gamma_\alpha+\Gamma_\beta)$, $\delta_2 = \sqrt{d_1 d_2}(\Gamma_\alpha-\Gamma_\beta)$ and $\phi = 2\sqrt{d_1 d_2}$. To allow the use of Theorem 6.5, Section 6.5.2 [9], we require that the random fluctuations have the form $m(x_3) = B(Y(x_3))$, where Y is a homogeneous in x_3 Markov process with values in the compact space $[0,\pi/2]\in\mathbb{R}$. We also assume that this process is strongly ergodic (the Markov process can traverse any part of the state space with a positive probability starting from anywhere in finite time), its infinitesimal generator satisfies the Fredholm alternative [4], and the real bounded function g satisfies the centring condition $\mathbb{E}[B(Y(0))] = 0$. Eq. (42) can be recast into an initial value problem associated with a propagator equation. That is

$$\begin{bmatrix}\hat{a}^\varepsilon(\omega,x_3)\\ \hat{b}^\varepsilon(\omega,x_3)\end{bmatrix} = \mathbf{P}^\varepsilon(\omega,x_3)\begin{bmatrix}\hat{a}^\varepsilon(\omega,0)\\ \hat{b}^\varepsilon(\omega,0)\end{bmatrix}, \tag{44}$$

where the propagator matrix

$$\mathbf{P}^\varepsilon(\omega,x_3) = \begin{bmatrix}\chi^\varepsilon(\omega,x_3) & \overline{\varkappa^\varepsilon}(\omega,x_3)\\ \varkappa^\varepsilon(\omega,x_3) & \overline{\chi^\varepsilon}(\omega,x_3)\end{bmatrix}, \tag{45}$$

is formed from solutions of Eq. (42) with initial condition $\mathbf{P}^\varepsilon(\omega,x_3=0) = \mathbf{I}$, that is $\chi^\varepsilon(\omega,0) = 1$ and $\overline{\varkappa^\varepsilon}(\omega,0) = 0$. The determinant of the propagator matrix is the conserved quantity $|\chi^\varepsilon|^2 - |\varkappa^\varepsilon|^2 = 1$.

4.1. Diffusion approximation theorem

To proceed we now apply the diffusion-approximation theorem in its linear form [9] to obtain the asymptotic distribution of the propagator matrix $\mathbf{P}^\varepsilon$. Use of the limit theorem shows that $\mathbf{P}^\varepsilon$ converges in distribution to $\mathbf{P}$ which is the solution of a stochastic differential equation. We write Eq. (44) using the propagator formulation (taking partial derivates in x_3 of Eq. (44) and substituting Eq. (42) to obtain the random matrix equation)

$$\frac{d\mathbf{P}^\varepsilon}{dx_3}(\omega,x_3) = \frac{1}{\varepsilon}\mathbf{H}\left(\frac{x_3}{\varepsilon^2}, m\left(\frac{x_3}{\varepsilon^2}\right)\right)\mathbf{P}^\varepsilon(\omega,x_3). \tag{46}$$

Splitting this into its real and imaginary parts gives

$$\begin{aligned}\frac{d\mathbf{P}^\varepsilon}{dx_3}(\omega,x_3) = {}& \frac{i}{2\varepsilon}m\left(\frac{x_3}{\varepsilon^2}\right)\delta_1\boldsymbol{\sigma}_3\mathbf{P}^\varepsilon(\omega,x_3)\\ & - \frac{1}{2\varepsilon}m\left(\frac{x_3}{\varepsilon^2}\right)\delta_2\sin\left(\frac{\phi x_3}{\varepsilon^2}\right)\boldsymbol{\sigma}_1\mathbf{P}^\varepsilon(\omega,x_3)\\ & + \frac{1}{2\varepsilon}m\left(\frac{x_3}{\varepsilon^2}\right)\delta_2\cos\left(\frac{\phi x_3}{\varepsilon^2}\right)\boldsymbol{\sigma}_2\mathbf{P}^\varepsilon(\omega,x_3),\end{aligned} \tag{47}$$

where $\boldsymbol{\sigma}_1,\boldsymbol{\sigma}_2,\boldsymbol{\sigma}_3$ are the Pauli spin matrices, defined as

$$\boldsymbol{\sigma}_1 = \begin{bmatrix}0 & 1\\ 1 & 0\end{bmatrix},\ \boldsymbol{\sigma}_2 = \begin{bmatrix}0 & -i\\ i & 0\end{bmatrix},\ \boldsymbol{\sigma}_3 = \begin{bmatrix}1 & 0\\ 0 & -1\end{bmatrix}. \tag{48}$$

The right hand side of Eq. (47) can be written as

$$\frac{1}{\varepsilon}\sum_{p=1}^{3} g^{(p)}(m(\tau),\tau)\,\mathbf{h}_p\mathbf{P}^\varepsilon, \tag{49}$$

where $\tau = x_3/\varepsilon^2$, $\mathbf{h}_1 = i\delta_1\boldsymbol{\sigma}_3/2$, $\mathbf{h}_2 = -\delta_2\boldsymbol{\sigma}_1/2$, $\mathbf{h}_3 = \delta_2\boldsymbol{\sigma}_2/2$ and $g^{(1)}(m,\tau) = m$, $g^{(2)}(m,\tau) = m\sin(\phi\tau)$, $g^{(3)}(m,\tau) = m\cos(\phi\tau)$. Recall that ϕ (defined below Eq. (43)) is independent of ω and is a function of $\rho, c_3, \bar{\theta}, \nu$ and the five independent stiffness tensor coefficients in Eq. (2). To use the diffusion approximation theorem (Theorem 6.4

in [9]), we need the correlation integral matrix $\mathbf{C} = (C_{pq})_{p,q=1,2,3}$. This can be computed using the covariance of the random process m (see Section 6.7.1 in [9]). The correlation matrix $\mathbf{C}$ can be written

$$\mathbf{C} = \begin{bmatrix} \Upsilon(0) & 0 & 0 \\ 0 & \frac{1}{2}\Upsilon(\phi) & -\frac{1}{2}\Upsilon^{AS}(\phi) \\ 0 & \frac{1}{2}\Upsilon^{AS}(\phi) & \frac{1}{2}\Upsilon(\phi) \end{bmatrix}, \tag{50}$$

where

$$\Upsilon(\phi) = 2\int_0^\infty \mathbb{E}\Big[m(0)m(x_3)\Big]\cos(\phi x_3)\,dx_3, \tag{51}$$

$$\Upsilon^{AS}(\phi) = 2\int_0^\infty \mathbb{E}\Big[m(0)m(x_3)\Big]\sin(\phi x_3)\,dx_3. \tag{52}$$

The quantity $\Upsilon(\phi)$ is a non-negative real number, and is proportional to the power spectral density of the stationary random process m (the Fourier cosine transform of the autocorrelation function at frequency zero; we refer to Section 6.3.6 in [9]). The symmetric (S) and anti-symmetric (AS) elements can be assembled in separate matrices as

$$\mathbf{C}^S = \begin{bmatrix} \Upsilon(0) & 0 & 0 \\ 0 & \frac{1}{2}\Upsilon(\phi) & 0 \\ 0 & 0 & \frac{1}{2}\Upsilon(\phi) \end{bmatrix}, \quad \mathbf{C}^{AS} = \begin{bmatrix} 0 & 0 & 0 \\ 0 & 0 & -\frac{1}{2}\Upsilon^{AS}(\phi) \\ 0 & \frac{1}{2}\Upsilon^{AS}(\phi) & 0 \end{bmatrix}. \tag{53}$$

Now the diffusion approximation (Theorem 6.4 in [9]) can be used to show that $\mathbf{P}^\varepsilon(\omega, x_3)$ converges in distribution to $\mathbf{P}(\omega, x_3)$ and satisfies the Stratonovich stochastic differential equation

$$d\mathbf{P}(\omega, x_3) = \sum_{l=1}^{3} \tilde{\mathbf{h}}_l \mathbf{P}(\omega, x_3) \circ dW_l(x_3) + \frac{1}{2}\sum_{p,q=1}^{3} \mathbf{C}_{pq}^{(AS)} \mathbf{h}_q \mathbf{h}_p \mathbf{P}(\omega, x_3) dx_3, \tag{54}$$

where $(\circ)$ denotes the Stratonovich integral. Note here that

$$\tilde{\mathbf{h}}_l = \sum_{p=1}^{3} \tilde{\sigma}_{lp}\mathbf{h}_p, \quad \tilde{\sigma}_{lp} = (\mathbf{C}_{lp}^S)^{1/2}, \tag{55}$$

and $W_l(x_3)$ are independent standard Brownian motions. Eq. (47) can be expanded to give

$$\begin{aligned} d\begin{bmatrix} \chi(\omega, x_3) & \overline{\varkappa}(\omega, x_3) \\ \varkappa(\omega, x_3) & \overline{\chi}(\omega, x_3) \end{bmatrix} &= iA_1 \begin{bmatrix} 1 & 0 \\ 0 & -1 \end{bmatrix} \begin{bmatrix} \chi(\omega, x_3) & \overline{\varkappa}(\omega, x_3) \\ \varkappa(\omega, x_3) & \overline{\chi}(\omega, x_3) \end{bmatrix} \circ dW_1(x_3) \\ &\quad - A_2 \begin{bmatrix} 0 & 1 \\ 1 & 0 \end{bmatrix} \begin{bmatrix} \chi(\omega, x_3) & \overline{\varkappa}(\omega, x_3) \\ \varkappa(\omega, x_3) & \overline{\chi}(\omega, x_3) \end{bmatrix} \circ dW_2(x_3) \\ &\quad + iA_2 \begin{bmatrix} 0 & -1 \\ 1 & 0 \end{bmatrix} \begin{bmatrix} \chi(\omega, x_3) & \overline{\varkappa}(\omega, x_3) \\ \varkappa(\omega, x_3) & \overline{\chi}(\omega, x_3) \end{bmatrix} \circ dW_3(x_3) \\ &\quad - iA_3 \begin{bmatrix} 1 & 0 \\ 0 & -1 \end{bmatrix} \begin{bmatrix} \chi(\omega, x_3) & \overline{\varkappa}(\omega, x_3) \\ \varkappa(\omega, x_3) & \overline{\chi}(\omega, x_3) \end{bmatrix} dx_3, \end{aligned} \tag{56}$$

where $A_1 = \delta_1\sqrt{\Upsilon(0)}/2$, $A_2 = \delta_2\sqrt{\Upsilon(\phi)}/(2\sqrt{2})$ and $A_3 = \delta_2^2\Upsilon^{AS}(\phi)/8$, with initial conditions $\chi(\omega, x_3 = 0) = 1$ and $\varkappa(\omega, x_3 = 0) = 0$.

4.2. Parameterising solution on a hyperbola

We follow a similar treatment to that in [9] (chapter 7) and parameterise the entries of the propagator matrix via

$$\chi(\omega, x_3) = \cosh\left(\frac{\gamma_\omega(x_3)}{2}\right) e^{i\phi_\omega(x_3)}, \tag{57}$$

$$\varkappa(\omega, x_3) = \sinh\left(\frac{\gamma_\omega(x_3)}{2}\right) e^{i(\phi_\omega(x_3)+\psi_\omega(x_3))}, \tag{58}$$

where $\gamma_\omega(x_3) \in [0, \infty)$, $\phi_\omega(x_3)$, $\psi_\omega(x_3) \in \mathbb{R}$, and $\gamma_\omega(x_3 = 0) = \phi_\omega(x_3 = 0) = \psi_\omega(x_3 = 0) = 0$. Eq. (56) can be converted to Itô form by calculating the modified drift [13] to give

$$d\gamma_\omega = -2A_2\Big(\cos(\psi_\omega)dW_2 - \sin(\psi_\omega)dW_3\Big) + \frac{2A_2^2}{\tanh(\gamma_\omega)}dx_3, \tag{59}$$

$$d\psi_\omega = \frac{2A_2}{\tanh(\gamma_\omega)}\Big(\cos(\psi_\omega)dW_3 + \sin(\psi_\omega)dW_2\Big) - 2A_1dW_1 + 2A_3\,dx_3, \tag{60}$$

and

$$d\phi_\omega = -A_2 \tanh(\gamma_\omega/2)\Big(\sin(\psi_\omega)dW_2 + \cos(\psi_\omega)dW_3\Big) + A_1 dW_1 - A_3\, dx_3. \tag{61}$$

This system can be reduced further by introducing two (auxiliary) random processes via

$$\begin{bmatrix} W_4 \\ W_5 \end{bmatrix} = \int_0^{x_3} \begin{bmatrix} \cos(\psi_\omega) & \sin(\psi_\omega) \\ \sin(\psi_\omega) & -\cos(\psi_\omega) \end{bmatrix} d\begin{bmatrix} W_3 \\ W_2 \end{bmatrix}, \tag{62}$$

so that the system (59) to (61) can be transformed to give

$$d\begin{bmatrix} \phi_\omega \\ \psi_\omega \\ \gamma_\omega \end{bmatrix} = \begin{bmatrix} A_1 & -A_2\tanh(\gamma_\omega/2) & 0 \\ -2A_1 & 2A_2/\tanh(\gamma_\omega) & 0 \\ 0 & 0 & 2A_2 \end{bmatrix} \begin{bmatrix} dW_1 \\ dW_4 \\ dW_5 \end{bmatrix} + \begin{bmatrix} -A_3 \\ 2A_3 \\ 2A_2^2/\tanh(\gamma_\omega) \end{bmatrix} dx_3. \tag{63}$$

The infinitesimal generator [9] of the Markov process $(\gamma_\omega,\ \phi_\omega,\ \psi_\omega)$ can be calculated as

$$\begin{aligned} \mathcal{L}_{\gamma_\omega,\phi_\omega,\psi_\omega} &= 2A_2^2\left[\frac{\partial^2}{\partial\gamma_\omega^2} + \frac{1}{\tanh(\gamma_\omega)}\frac{\partial}{\partial\gamma_\omega}\right] \\ &\quad + A_2^2\left[\frac{1}{2}\tanh^2(\gamma_\omega/2)\frac{\partial^2}{\partial\phi_\omega^2} - 2\frac{\tanh(\gamma_\omega/2)}{\tanh(\gamma_\omega)}\frac{\partial^2}{\partial\phi_\omega\partial\psi_\omega} + \frac{2}{\tanh^2(\gamma_\omega)}\frac{\partial^2}{\partial\psi_\omega^2}\right] \\ &\quad + A_1^2\left[\frac{1}{2}\frac{\partial^2}{\partial\phi_\omega^2} - 2\frac{\partial^2}{\partial\phi_\omega\partial\psi_\omega} + 2\frac{\partial^2}{\partial\psi_\omega^2}\right] \\ &\quad + A_3\left[2\frac{\partial}{\partial\psi_\omega} - \frac{\partial}{\partial\phi_\omega}\right]. \end{aligned} \tag{64}$$

The radial process γ_ω (so focusing on the amplitude in transformations (57) and (58)) has infinitesimal generator

$$\mathcal{L}_{\gamma_\omega} = \frac{\delta_2^2\Upsilon(\phi)}{4}\left(\frac{\partial^2}{\partial\gamma_\omega^2} + \frac{1}{\tanh(\gamma_\omega)}\frac{\partial}{\partial\gamma_\omega}\right). \tag{65}$$

The boundary conditions for Eq. (44) are prescribed by $\hat{a}(\omega, x_3 = 0) = 1, \quad \hat{b}(\omega, x_3 = L) = 0$, and $\hat{b}(\omega, x_3 = L) = 0$ which translates into a unit wave travelling from the left and no left-going wave from the right at $x_3 = L$. The reflection and transmission coefficients are given by $R_\omega(\omega, L) = \hat{b}(\omega, 0)$ and $T_\omega = \hat{a}(\omega, L)$. Using Eq. (44), we have the system

$$\begin{bmatrix} \hat{a}(\omega, L) \\ \hat{b}(\omega, L) \end{bmatrix} = \begin{bmatrix} T_\omega(L) \\ 0 \end{bmatrix} = \mathbf{P}(\omega, L)\begin{bmatrix} 1 \\ R_\omega(L) \end{bmatrix}. \tag{66}$$

That is

$$R_\omega(\omega, L) = -\frac{\varkappa(\omega, L)}{\overline{\chi}(\omega, L)}, \quad \text{and} \quad T_\omega(\omega, L) = \frac{1}{\overline{\chi}(\omega, L)}. \tag{67}$$

4.3. Deriving localisation length from transmission coefficient

Proposition 1. *The random process γ_ω satisfies*

$$\frac{1}{\cosh(\gamma_\omega(L)/2)} = \exp -A_2\int_0^L \tanh(\gamma_\omega(x_3)/2)dW_5(x_3) - A_2^2 L. \tag{68}$$

Proof. We define the power transmission coefficient (using Eqs. (57) and (67)) to be

$$\tau(L) = |T_\omega(\omega, L)|^2 = \cosh^{-2}\left(\frac{\gamma_\omega(L)}{2}\right), \tag{69}$$

which describes the amplitude of the energy transmitted through the medium. Using Eq. (68) we can write

$$\tau(x_3) = \exp -2A_2\int_0^L \tanh(\gamma_\omega(x_3)/2)dW_5(x_3) - 2A_2^2 L. \tag{70}$$

Integrating Eq. (61) we obtain

$$\phi_\omega(L) = A_1 W_1(L) - A_2\int_0^L \tanh(\gamma_\omega(x_3)/2)dW_4(x_3) - A_3 L, \tag{71}$$

so that we may write

$$\exp i\phi_\omega(L) = \exp iA_1 W_1(L) - iA_2\int_0^L \tanh(\gamma_\omega(x_3)/2)dW_4(x_3) - iA_3 L. \tag{72}$$

Since $d(\cosh(\gamma_\omega/2)^{-1}) = -1/2(\tanh(\gamma_\omega/2)/\cosh(\gamma_\omega/2)) \circ d\gamma_\omega$, then Eq. (63) gives

$$d(\cosh(\gamma_\omega/2)^{-1}) = -\frac{1}{2}\left(\frac{\tanh(\gamma_\omega/2)}{\cosh(\gamma_\omega/2)}\right) \circ \left(2A_2 dW_5 + \frac{2A_2^2}{\tanh(\gamma_\omega)}dx_3\right). \tag{73}$$

Multiplying both sides by $\cosh(\gamma_\omega/2)$, introducing $Z(x_3)$ for brevity and integrating with respect to x_3 (from 0 to L) we obtain

$$\begin{aligned} Z(L) = \ln(\cosh(\gamma_\omega(L)/2)^{-1}) = -A_2 \int_0^L \tanh(\gamma_\omega(x_3)/2) \circ dW_5(x_3) \\ - A_2^2 \int_0^L \frac{\tanh(\gamma_\omega(x_3)/2)}{\tanh(\gamma_\omega(x_3))} dx_3. \end{aligned} \tag{74}$$

Since $\tanh^2(\gamma_\omega/2) = 1 - \cosh^{-2}(\gamma_\omega/2) = 1 - \tau_\omega = 1 - e^{2Z(x)}$, then

$$Z(L) = -A_2 \int_0^L \left(1 - e^{2Z(x_3)}\right)^{\frac{1}{2}} \circ dW_5(x_3) - \frac{A_2^2}{2}\int_0^L \left(2 - e^{2Z(x_3)}\right) dx_3. \tag{75}$$

where we have used the identity $\tanh(\gamma_\omega/2)/\tanh(\gamma_\omega) = 1/2(1 + \tanh(\gamma_\omega/2)^2) = 1/2(2 - \tau_\omega) = 1/2(2 - e^{2Z(x_3)})$. We convert Eq. (75) into Itô form to obtain

$$Z(L) = -A_2 \int_0^L (1 - e^{2Z(x_3)})^{\frac{1}{2}} dW_5(x_3) - A_2^2 L. \tag{76}$$

Taking exponentials of both sides (and using Eq. (74)) we can then obtain Eq. (68) which completes the proof. □

Proposition 2. *The natural logarithm of the transmission coefficient converges almost surely (when $L \to \infty$) as*

$$\lim_{L\to\infty} \frac{1}{L}\ln(\tau) = -\frac{1}{L_{loc}}, \quad \textit{where} \quad L_{loc} = \frac{1}{2A_2^2}. \tag{77}$$

Proof. From Eq. (70), since $\gamma_\omega(L) \to \infty$ as $L \to \infty$ we can write (almost surely) for large L

$$\tau(L) \sim \exp -2A_2^2 L - 2A_2 W_5(L) = \exp -\frac{2W_5(L)}{\sqrt{L_{loc}}} - \frac{L}{L_{loc}}, \tag{78}$$

where $L_{loc} = 1/(2A_2^2)$. Since $W_5(L)/L \to 0$ almost surely as $L \to \infty$, then

$$\lim_{L\to\infty} \frac{\ln(\tau)}{L} = -\frac{1}{L_{loc}}. \quad \square \tag{79}$$

The non-dimensionalised localisation length is written as

$$\tilde{L}_{loc}(\nu, c_{ijkl}, \rho, \theta(x_3)) = \frac{L_{loc}}{L_3} = \frac{1}{2\tilde{A}_2^2 L_3} = \frac{4}{\delta_2^2 \tilde{\Upsilon}(\phi)} = \frac{4}{\delta_2^2(\nu, c_{ijkl}, \rho)\tilde{\Upsilon}(\nu, c_{ijkl}, \rho, \theta(x_3))}, \tag{80}$$

where $\tilde{\Upsilon}(\phi) = \Upsilon(\phi)/L_3$ is the non-dimensional correlation integral. This non-dimensional parameter $\tilde{L}_{loc}$ controls the rate of the decay of energy through the random slab. □

4.4. Fokker–Planck equation for the power transmission coefficient

Proposition 3. *The moments of the power transmission coefficient can be written as*

$$\mathbb{E}[\tau^n(L)] = e^{-\frac{L}{4L_{loc}(\nu)}} \int_0^\infty \frac{2\pi\mu\sinh(\mu\pi)}{\cosh^2(\mu\pi)} e^{-\frac{\mu^2 L}{L_{loc}(\nu)}} K^{(n)}(\mu) d\mu, \tag{81}$$

where

$$K^{(n)}(\mu) = \prod_{j=1}^{n-1} \frac{1}{j^2}\left(\mu^2 + \left(j - \frac{1}{2}\right)^2\right), \quad K^{(1)}(\mu) = 1. \tag{82}$$

Proof.

From Eqs. (65) and (69) the infinitesimal generator of the power transmission coefficient can be written (dropping tildes) as

$$\mathcal{L}_\tau = \frac{1}{L_{loc}}\left(\tau^2(1-\tau)\frac{\partial^2}{\partial\tau^2} - \tau^2\frac{\partial}{\partial\tau}\right). \tag{83}$$

Introducing the transformation $\eta = (2-\tau)/\tau$, which takes values in $[1, \infty)$, the infinitesimal generator is given by

$$\mathcal{L}_\eta = \frac{1}{L_{loc}} \frac{\partial}{\partial \eta} \left((\eta^2 - 1) \frac{\partial}{\partial \eta} \right). \tag{84}$$

The operator $\mathcal{L}_\eta$ is self adjoint and hence, the Fokker–Planck equation for the probability density function of $\eta(x_3 = L)$ is

$$\frac{\partial p}{\partial L}(L, \eta) = \frac{1}{L_{loc}} \frac{\partial}{\partial \eta} \left(\eta^2 - 1 \right) \frac{\partial p}{\partial \eta}(L, \eta), \quad \eta > 1, \tag{85}$$

with initial condition $p(L = 0, \eta) = \delta(\eta - 1)$, where δ denotes the Dirac delta function. This can be solved analytically by the use of the Mehler–Fock transform [9,19] to give the probability density function (PDF) of the process $\eta(L)$

$$p(L, \eta) = \int_0^\infty \mu \tanh(\mu\pi) P_{-\frac{1}{2}+i\mu}(\eta) \exp - \left(\mu^2 + \frac{1}{4} \right) \frac{L}{L_{loc}} \, d\mu, \tag{86}$$

where $P_{-\frac{1}{2}+i\mu}(\eta)$ is the Legendre function of the first kind. Equipped with the probability density function for the power transmission coefficient, the moments of the power transmission coefficient are (we refer to [9] and in particular proposition 7.3 and Section 7.6.1) then given by Eqs. (81) and (82) which completes the proof. □

The SDE approach used in this study allows for analytical comment to be made about the probability distribution of the transmission amplitude via its moments. Of particular interest is the second moment as this captures the uncertainty in the estimate of the transmission coefficient amplitude. If this is large then it suggests that a homogenisation approach is not appropriate as each different realisation of the heterogeneous material will give a very different transmitted wave amplitude. Conversely, when it is a narrow probability density function, that is when the second moment is small due to self-averaging, and this would suggest that homogenisation could be used. One can see in Fig. 4 that for say $\nu = 0.5$ then for a large enough propagation distance the second moment is small enough for a homogenisation approach to be applicable. This ability to measure the uncertainty in the ultrasonic nondestructive testing of such materials is of practical interest to engineers who may wish to design the inspection of a component to reduce uncertainty.

4.5. Moments of the power reflection coefficient

A similar calculation can be performed for the reflection coefficient (as defined in Eq. (67)). Using Eqs. (57) and (58) then

$$R_\omega(\omega, L) = -\tanh(\gamma_\omega(L))/2 e^{i(\psi_\omega(L) + 2\phi_\omega(L))}, \tag{87}$$

the reflected energy is defined as

$$|R_\omega(\omega, L)|^2 = \tanh^2(\gamma_\omega(L)/2) = R, \tag{88}$$

say. Using the chain rule, the infinitesimal generator (see Section 6.6.3 in [9] for details) for the power reflection coefficient R reads

$$\mathcal{L}_R = \frac{1}{L_{loc}} \left[R(1-R)^2 \frac{\partial^2}{\partial R^2} + (1-R)^2 \frac{\partial}{\partial R} \right]. \tag{89}$$

Using $v = (1+R)/(1-R)$ and $R = (v-1)/(v+1)$, the infinitesimal generator is then

$$\mathcal{L}_v = \frac{1}{L_{loc}} \frac{\partial}{\partial v} \left[(v^2 - 1) \frac{\partial}{\partial v} \right], \tag{90}$$

which is self-adjoint. The Fokker–Planck equation for the probability density function of the power reflection coefficient $p(L, v)$ then reads

$$\frac{\partial p}{\partial L}(L, v) = \frac{1}{L_{loc}} \frac{\partial}{\partial v} \left[(v^2 - 1) \frac{\partial p}{\partial v}(L, v) \right], \quad v > 1, \tag{91}$$

with initial condition $p(L = 0, v) = \delta(v - 1)$, where δ denotes the Dirac delta function. Note that this is the same form of Fokker–Planck equation as seen in Eq. (85) in the analysis of the power transmission coefficient. Using the solution for the probability density function of the power transmission coefficient (Eq. (86)) the moments of the power reflection coefficient are given by

$$\mathbb{E}[R^n(L)] = \int_0^1 R^n(L) p(L, R) \, dR = \int_1^\infty \left(\frac{v-1}{v+1} \right)^n p(L, v) \, dv. \tag{92}$$

Starting with the first moment ($n = 1$) we obtain

$$\mathbb{E}[R(L)] = \int_1^\infty \left(\frac{v-1}{v+1} \right) p(L, v) \, dv = \int_1^\infty \left(1 - \frac{2}{v+1} \right) p(L, v) \, dv = 1 - \int_1^\infty \left(\frac{2}{1+v} \right) p(L, v) \, dv. \tag{93}$$

Table 1
Table of material constants for a CFRP obtained from IHI corporation (private communication) with geometry [17].

	Elastic material constants (in GPa)($\mathrm{ML^{-1}T^{-2}} \times 10^9$)					
	C_{11}	C_{33}	C_{44}	C_{66}	C_{13}	Density (ρ)(kg $\mathrm{m^{-3}}$)
CFRP	146.53	12.25	2.55	4.00	6.67	1550

The second integral term is precisely the integral we solved in the transmission case. Thus Eq. (81) gives $\mathbb{E}[R(L)] = 1 - \mathbb{E}[\tau(L)]$, and so $\mathbb{E}[\tau(L)] + \mathbb{E}[R(L)] = 1$, and energy is conserved. Now moving to the second moment ($n = 2$) we obtain

$$\begin{aligned}\mathbb{E}[R^2(L)] &= \int_1^\infty \left(\frac{v-1}{v+1}\right)^2 p(L,v)\,dv = \int_1^\infty \left(1 - \frac{2}{v+1}\right)^2 p(L,v)\,dv \\ &= \int_1^\infty p(L,v)\,dv + \int_1^\infty \left(\frac{2}{1+v}\right)^2 p(L,v),\ dv - 2\int_1^\infty \left(\frac{2}{1+v}\right) p(L,v)\,dv \\ &= 1 + \mathbb{E}[\tau^2(L)] - 2\mathbb{E}[\tau(L)]. \end{aligned} \tag{94}$$

Note that standard deviation of the reflected energy

$$\begin{aligned}\mathrm{Std}[R(L)] &= \sqrt{\mathbb{E}[R^2(L)] - \mathbb{E}[R(L)]^2} = \sqrt{1 + \mathbb{E}[\tau^2(L)] - 2\mathbb{E}[\tau(L)] - (1 - \mathbb{E}[\tau(L)])} \\ &= \sqrt{\mathbb{E}[\tau^2(L)] - \mathbb{E}[\tau(L)]^2} = \mathrm{Std}[\tau(L)], \end{aligned} \tag{95}$$

is equal to the standard deviation of the transmitted energy.

5. Numerical results

5.1. Numerical calculation of correlation integrals

For illustrative purposes, we simulate a material in order to show how the correlation matrix components (51) and (52) can be computed via quadrature. The symmetric correlation integral $\Upsilon(\phi)$ may be written in discretised form as

$$\Upsilon_N(\phi) = 2\sum_{i=1}^{N}\left(\sum_{r=1}^{R}\sum_{j=1}^{K}\frac{(m_1^r)^j(m_i^r)^j}{RK}\right)\cos(\phi x_3^i)\Delta x_3, \tag{96}$$

where $(m_i^r)^j$ is the orientation of the anisotropic material in realisation j, along ray r and at arc length position $(x_3)^i$. These orientations are drawn from a uniform distribution over $[-1, 1]$. The mean layer size $l = \lambda_3$ is chosen accordingly so that we are in the weakly heterogeneous regime $L_3 \gg \lambda_3 \sim l$. We assume that the layer sizes

$$(X_1, X_2 - X_1, \ldots, X_n - X_{n-1}, \ldots), \tag{97}$$

constitute a sequence of independent random variables following an exponential distribution with rate $1/l$

$$\mathbb{P}[X_n - X_{n-1} \le x_3] = 1 - e^{-x_3/l}. \tag{98}$$

This ensures that the layer lengths are constructed according to an exponential distribution and therefore form a Markov process [9]. Since we are working in a scaled non-dimensional framework, our propagation distance is denoted by $\tilde{L}$ and $l = 1$. Typical values of the correlation integrals are of order one. Note that $\Upsilon(\phi)$ is a non-negative real number (which is expected) since it is proportional to the power spectral density of the random process m [13].

Carbon fibre reinforced polymers (CFRP's) are a common class of materials in the engineering world and have material properties that align with our model; specifically the heterogeneous and locally anisotropic nature of layered CFRP's. For our study a frequency of $f = 1\,\mathrm{MHz}$ ($\tilde{\omega} \sim \varepsilon^{-2}$) and a mean wave speed of $c_3 = 2000\,\mathrm{m\ s^{-1}}$ were used together with the elastic constants in Table 1.

We analyse the mean power transmission coefficient given by Eq. (81) as a function of key parameters, including the propagation distance $\tilde{L}$ through the material and $\nu = \kappa_1/\kappa_3$ which controls the direction of the wave through the layered medium. The decrease in $\tilde{L}_{loc}$ (see Eq. (80)) as the wavefront direction ν increases is shown in Fig. 2. Increasing the wavenumber in the x_1 direction and keeping the wavenumber in the x_3 direction fixed, increases the angle of incidence of the wave and leads to a longer travel distance through the layers corresponding to greater multiple scattering through each layer. This change in the localisation length ($\tilde{L}_{loc}$) affects the decay rate of the mean power transmission coefficient $\mathbb{E}[\tau(\tilde{L}, \nu)]$ (Eq. (81)) as shown in Fig. 3. An increase in the ratio of wave numbers (directivity of the wave) causes greater energy decay with the depth of wave penetration into the material $\tilde{L}$.

We also see the effect of changing the wave direction (ν) on the standard deviation of the power transmission coefficient. Fig. 4 shows the narrowing of the peak of the standard deviation of the power transmission coefficient as ν increases and the self-averaging of the wave for large propagation distance $\tilde{L}$.

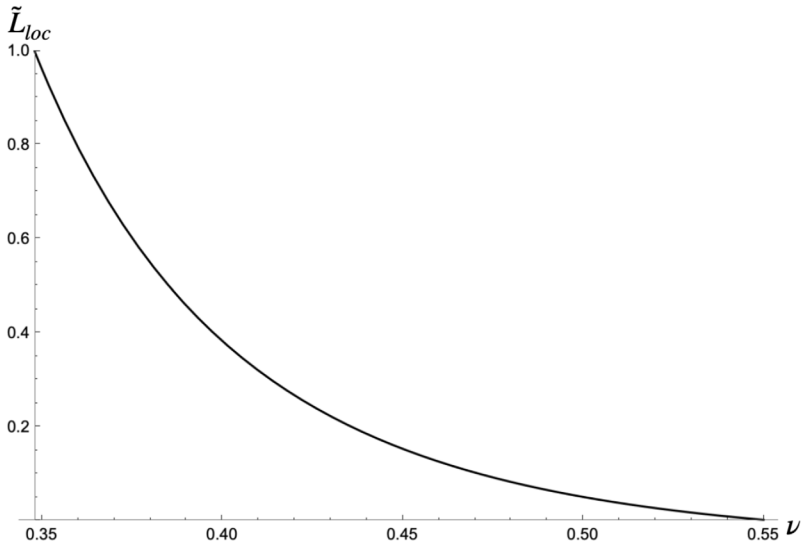

Fig. 2. Non-dimensional localisation length $\tilde{L}_{loc}$ (given by Eq. (80)) as a function of the wave directivity parameter ν (Eq. (33)). The material properties are given in Table 1.

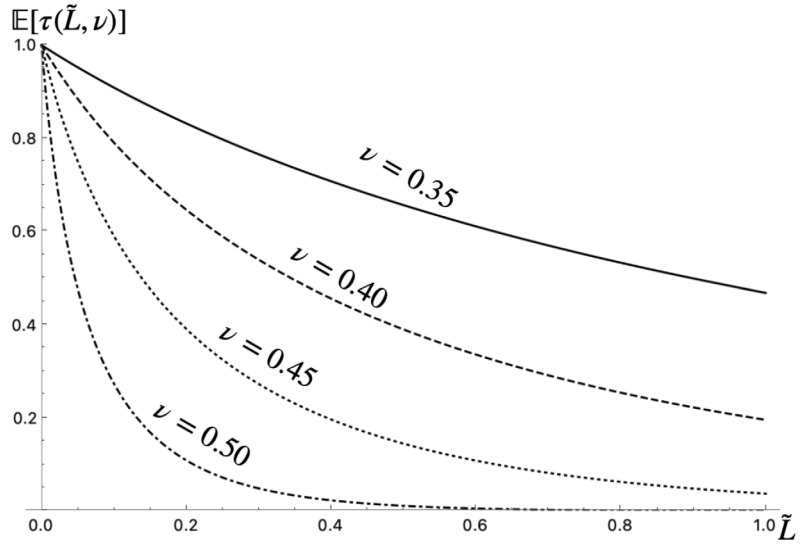

Fig. 3. Plots of the mean of the power transmission coefficient (see Eq. (81)) as the non-dimensionalised penetration depth $\tilde{L}$ varies for different values of the wave directivity parameter ν (Eq. (33)). The material properties are given in Table 1.

6. Conclusion

A model of a monochromatic horizontally polarised shear wave propagating through a randomly layered heterogeneous medium composed of a locally anisotropic material has been constructed. A suitable scaling regime was studied whereby the microstructure produced a transmitted wave which had an attenuated, coherent wave front followed by an incoherent coda wave. We modelled the random fluctuations present within the anisotropic material via a local rotation of the corresponding slowness surface as a function of the wave propagation direction (x_3). We obtained a system of stochastic differential equations which we solved in order to access the statistical properties of the energy transmitted and reflected through this layered random medium.

A horizontally polarised shear wave parameterisation $\mathbf{u} = (0, u_2(x_1, x_3), 0)$ was chosen and the transmitted energy (attenuation) of the amplitude of the coherent wave then depended on the direction of the wave vector in the (x_1, x_3) plane. This variation in the wave attenuation on the direction of propagation ($\nu = \kappa_1/\kappa_3$) has relevance to the use of ultrasonic arrays for medical imaging and nondestructive testing applications [14,20]. We have also derived an expression

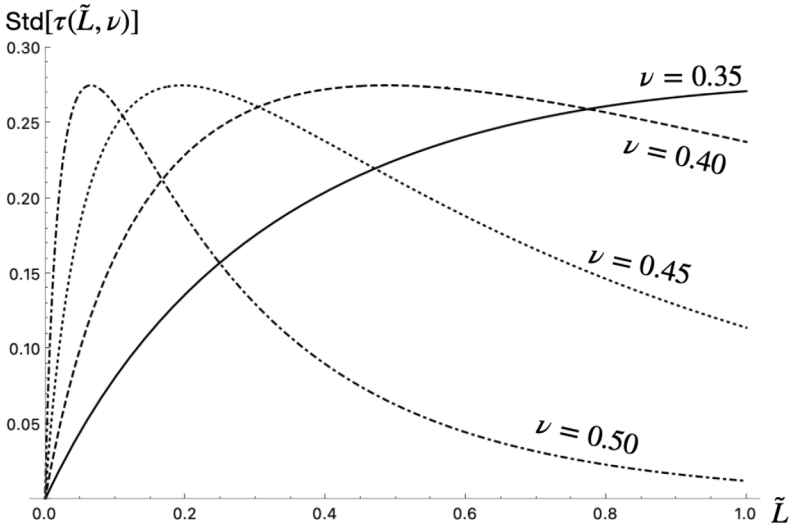

Fig. 4. Plots of the standard deviation of the power transmission coefficient (Eq. (81)) as the non-dimensionalised wave propagation depth $\tilde{L}$ varies for different values of the wave directivity parameter ν (Eq. (33)). The material properties are given in Table 1.

for the localisation length, which depends on correlation integrals which can be numerically evaluated for specific material microstructures. It was found that the wave direction had a significant effect on the depth of penetration of the wave as characterised by the localisation length L_{loc}. For example, a 20% change in the wave direction could lead to a threefold reduction in the amplitude of the transmitted coherent wave. The work presented here could be used by experimentalists to decide on an appropriate frequency of ultrasonic wave to emit for a given material microstructure and required depth of wave penetration.

CRediT authorship contribution statement

Alistair S. Ferguson: Conceptualization, Methodology, Simulations, Writing, Reviewing, Editing. **Anthony J. Mulholland:** Conceptualization, Methodology, Reviewing. **Katherine M.M. Tant:** Conceptualization, Methodology, Reviewing. **Mohammud Foondun:** Conceptualization.

Declaration of competing interest

The authors declare that they have no known competing financial interests or personal relationships that could have appeared to influence the work reported in this paper.

Data availability

Data will be made available on request.

Acknowledgements

This work was supported by a studentship from the National Physical Laboratory (NPL) and the University of Strathclyde. This work was also supported by EPSRC, grant number EP/S001174/1. The authors thank Professor Alistair Forbes (National Physical Laboratory, UK) and Professor Knut Sølna (University of California at Irvine) for discussions and references.

References

[1] B. Raj, T. Jayakumar, B.P.C. Rao, Non-destructive testing and evaluation for structural integrity, Integr. Eng. Compon. 20 (1995) 5–38.
[2] B.W. Drinkwater, P.D. Wilcox, Ultrasonic arrays for non-destructive evaluation: A review, NDT E Int. 39 (7) (2006) 525–541.
[3] C. Li, D. Pain, P.D. Wilcox, B.W. Drinkwater, Imaging composite material using ultrasonic arrays, NDT E Int. 53 (2013) 8–17.
[4] J. Garnier, K. Sølna, Apparent attenuation of shear waves propagating through a randomly anisotropic medium, Stoch. Dyn. 16 (4) (2015).
[5] I.D. Abrahams, G.R. Wickham, The propagation of elastic waves in a certain class of inhomogeneous anisotropic materials. I. The refraction of a horizontally polarized shear wave source, Lond., R. Soc. Publishing 14 (1898) (2006).
[6] R.B. Thompson, F.J. Margetan, P. Haldipur, L. Yu, A. Li, P. Panetta, H. Wasan, Scattering of elastic waves in simple and complex polycrystals, Wave Motion 45 (5) (2008) 655–674.

[7] J. Hunt, M. Arditi, F.S. Foster, Ultrasound transducers for pulse-echo medical imaging, IEEE Trans. Biomed. Eng. BME-30 (8) (1983) 453–481.
[8] M.V. de Hoop, A.T. de Hoop, Elastic wave up/down decomposition in inhomogeneous and anisotropic media: an operator approach and its approximations, Wave Motion 20 (1) (1994) 57–82.
[9] J. Fouque, J. Garnier, G. Papanicolaou, K. Sølna, Wave Propagation and Time Reversal in Randomly Layered Media, New York, Springer, 2007.
[10] G.C. Papanicolaou, Wave propagation in a one-dimensional random medium, SIAM J. Appl. Math. 21 (1) (1971).
[11] G. Papanicolaou, S. Weinryb, A functional limit theorem for waves reflected by a random medium, Appl. Math. Optim. 30 (1994) 307–334.
[12] J. Garnier, K. Sølna, Parabolic and white-noise approximations for elastic waves in random media, Wave Motion 46 (4) (2009) 237–254.
[13] R.F. Bass, Stochastic processes, in: Cambridge Series in Statistical and Probabilistic Mathematics, Cambridge University Press, 2011.
[14] G. Harvey, A. Tweedie, C. Carpentier, P. Reynolds, Finite element analysis of ultrasonic phased array inspections on anisotropic welds, in: AIP Conf Proc, San Diego, California, Vol. 1335, 2010, pp. 827–834.
[15] J.D. Achenbach, Wave Propagation in Elastic Solids, North Holland, 1973.
[16] M. Spies, Elastic waves in homogeneous and layered transversely isotropic media: Plane waves and Gaussian wave packets. A general approach, J. Acoust. Soc. Am. 95 (1748) (1994).
[17] V. Munoz, M. Perrin, M. Pastor, H. Welemane, A. Cantarel, M. Karama, Determination of the elastic properties in CFRP composites: comparison of different approaches based on tensile tests and ultrasonic characterization, Adv. Aircraft Spacecraft Sci. 2 (3) (2015) 249–260.
[18] A. Ferguson, A.J. Mulholland, K.M.M. Tant, Modelling of ultrasonic waves in layered elastic heterogeneous materials, in: 2021 IEEE International Ultrasonics Symposium, IUS, 2021, pp. 1–4.
[19] V.A. Ditkin, A.P. Prudnikow, Integral Transforms and Operational Calculus, Pergamon Press, New York, 1965.
[20] C. Nageswaran, C. Carpentier, Y.Y. Tse, Microstructural quantification, modelling and array ultrasonics to improve the inspection of austenitic welds, Insight, Non-Destr. Test. Cond. Monit. 51 (12) (2009) 660–666.